Numerical and experimental investigation of axial fan with trailing edge self-induced blowing

Matjaž Eberlinc · Brane Širok · Marko Hočevar · Matevž Dular

Abstract Axial fans often show adverse flow conditions at the fan hub and at the tip of the blades. In the present paper, a modification of conventional axial fan blades with numerical and experimental investigation is presented. Hollow blades were manufactured from the hub to the trailing edge at the tip of the blades. They enable the formation of self-induced internal flow through internal passages. The internal flow enters the internal radial flow passages of the hollow blades through the openings near the fan hub and exits through the trailing edge slots at the tip of the blade. The study of the influence of internal flow on the flow field of axial fan and the modifications of aerodynamic characteristics of the axial fan have been made. The numerical and experimental results show a comparison of integral and local characteristics of the axial fan with the internal flow, compared to characteristics of a geometrically equivalent fan without internal flow. The experimental results of local characteristics were performed with a five-hole probe and computer-aided visualization. A reduction of adverse flow conditions near the trailing edge at the tip of the blade was achieved, as well as boundary layer reduction on the blade suction side and the reduction of flow separation. The introduction of self-induced blowing led to the preservation of the direction of external flow, defined by blade geometry, and enabled maximal local energy conversion. The integral characteristic reached higher degree of efficiency.

Keywords Axial fan · Hollow blade · Self-induced blowing · Numerical simulation · Five-hole probe · Computer-aided visualization

M. Eberlinc (✉) · B. Širok · M. Hočevar · M. Dular
Faculty of Mechanical Engineering, University of Ljubljana,
Aškerčeva 6,
1000 Ljubljana, Slovenia
e-mail: matjaz.eberlinc@fs.uni-lj.si

Numerische und messtechnische Untersuchung eines Axialventilators mit selbstverursachtem inneren Blasen

Zusammenfassung Axialventilatoren zeigen häufig ungünstigen Strömungszustand bei dem Zentrum des Ventilators und und den Schaufelstipzen. In diesem Artikel wird die Modifikation des konventionellen Ventilators mit Hilfe numerischer und messetechnischer Untersuchung präsentiert. Hohlschaufel des Axialventilators wurde vom Zentrum des Ventilators bis zu den Schaufelspitzen hergestellt. Hohlschaufel des Axialventilators ermöglicht das Entstehen des selbstverursachten inneren Blasens quer durch die innere Passage. Der innere Luftstrom tritt durch die innere radiale Passage der Hohlschaufel durch die Öffnung in der Nähe vom Zentrum des Ventilators ein und durch die Öffnung in der Nähe der Schaufelspitze aus. Die Erforschung des Einflusses des inneren Blasens auf das Axialventilatorluftstromfeld und die Modifikation von aerodynamischen Eigenschaften des Axialventilators wurden durchgeführt. Die numerischen und messtechnischen Ergebnisse stellen den Vergleich von integralen und lokalen Eigenschaften des Axialventilators mit innerem Luftstrom dar, und zwar mit den Eigenschaften des geometrisch äquivalenten Axialventilators ohne inneren Luftstrom. Die messtechnischen Ergebnisse von Lokalcharakteristiken waren mit der Fünf-Loch Sonde und mit computerunterstützter Visualisierung erlangt. Es wurde die Reduzierung des ungünstigen Zustands des Luftstroms in der Nähe der Schaufelspitze, die Reduzierung der Grenzschiechten und die Reduzierung der Grenzschichtablösung erreicht. Die Einführung des selbstverursachten inneren Blasens führte bis zu der Erhaltung der Luftströmungs-Richtung von externem Luftstrom, definiert mit der Schaufelgeometrie, und ermöglichte die maximale lokale Energieumsetzung. Die Integralcharakteristik erreichte eine größere Leistungsstufe.

🍥 Springer

List of Symbols

D	Diameter	mm
D_ω	Diffusive term	
E	Digital image element	–
$\tilde{G}_k$	Turbulence source	
G_ω	Velocity source	
k	Turbulent kinetic energy	
n	Fan rotation	min^{-1}
p	Pressure	Pa
u	Velocity	m/s
w	Relative velocity	m/s
q	Flow	m^3/h
v	Velocity	m/s
t	Time	s
Y_k	Dissipations of k	
Y_ω	Dissipations of ω	

Greek Letters

Δ	Difference	–
Γ_k	Effective diffusivity of k	
Γ_ω	Effective diffusivity of ω	
α	Angle	^{o}
ρ	Air density	kg/m^3
η	Normalized efficiency	–
ω	Specific dissipation	

Subscripts

j	Internal jet flow
p	Pixel
s	Static
v	Volume

1 Introduction

Axial fans often show adverse flow conditions at the fan hub and at the tip of the blades [4]. We present a method to reduce these adverse flow conditions by introducing hollow blades. The internal flow enters the hollow blade near the fan hub, and exits it as free jet at the trailing edge at the tip of the blade (Fig. 1a). The internal flow is self-induced as no additional energy is required and the only driving force is the fan rotation. The internal flow is mainly driven by the centrifugal forces resulting from the fan rotation. The internal flow passage is mainly radial while the flow exits in axial direction, although the direction of the internal flow is defined by the shape of the hollow blade (Fig. 1b). Using these modifications, we estimate to achieve the reduction of adverse flow conditions near the trailing edge at the tip of the blade, boundary layer reduction on the blade suction side and the reduction of flow separation, which will enable increased local energy conversion and improve fan characteristics [3, 12, 15, 21].

The concept of reducing blade wake through trailing edge blowing has been investigated in the literature, where different explanations were proposed. Schlichting [18] developed a method for preventing separation where additional energy is supplied to the particles of fluid. Suction was applied in the design of aircraft wings by Rhee et al. [17], where much larger maximum lift values were obtained. Garg [10] presented the use of hollow blades in gas turbine with induced secondary flow circulation where the purpose was blade cooling. Murthy et al. [16] experimentally and numerically described the system which is used in chemical industry for mixing of multi-phase fluids. In their study, the gas is supplied through the hollow impeller shaft. The gas continues

Fig. 1 Axial fan with self-induced trailing edge blowing, **a** scheme, **b** hollow blade
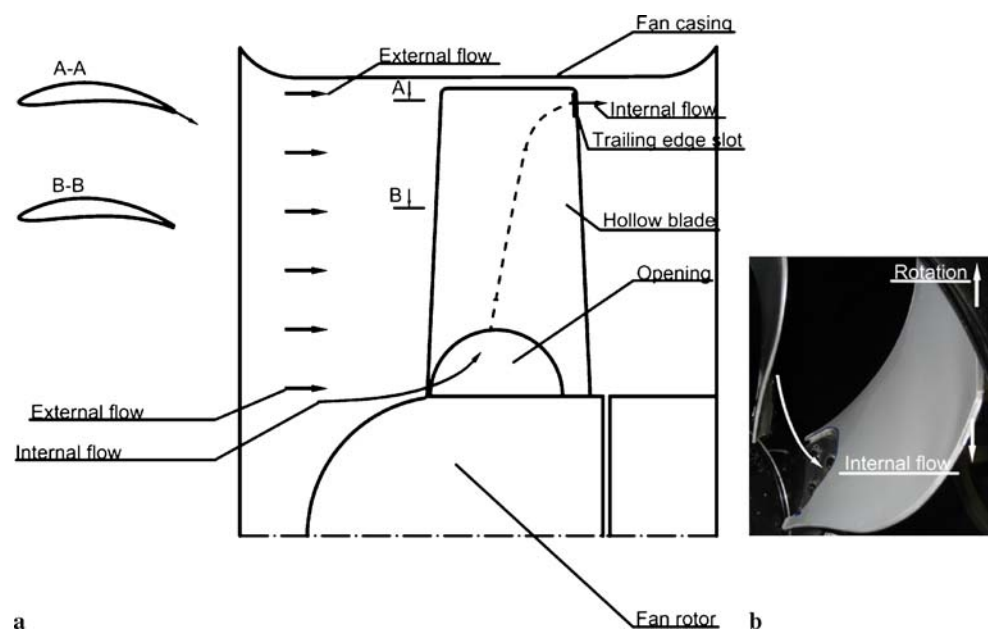
along to every individual blade, where exit slots on the impeller blades in low pressure regions are drilled. Gas mixes with external fluid and influences the flow field in the vicinity. Bleier [2] presented a $\varnothing$508 vane-axial fan wheel driven by compressed-air jets with a 31 per cent hub-tip ratio and four airfoil blades, where the compressed-air nozzles on two of the four blades were mounted on the inlet side, producing a high-velocity jet of compressed air, ejected through the opening at the trailing edge at the tip of the blade. Sutliff et al. [19] and Woodward et al. [22] presented turbofan noise reduction with full-span trailing edge blowing with hollow blades and internal flow in internal radial flow passages. From both authors, far-field acoustic results showed that full-span blowing near 2.0 per cent of the total flow could reduce the overall sound power level by about 2.0 dB.

We expect that external flow better follows the blade shape near the trailing edge at the tip of the blade and that the fan integral characteristic reaches a higher degree of static pressure difference.

Changes of flow field near the fan hub are also expected. They mostly result from the internal flow flowing into the internal radial flow passage; consequently, a reduction of radial flow in the cascade near the fan hub is expected.

To confirm the above assumptions, a comparison of two versions differing only in the presence or the absence of blade internal flow was investigated. Numerically supported CFD method was used, which enabled predictions of machine's integral characteristic and local flow properties. Measurements of the aerodynamic characteristic and efficiency were performed. Both versions were compared by experimental analysis of local velocity field measurements with a five-hole probe. In addition to the experimental measurements of local characteristics, a method based on computer-aided visualization was used. This allowed the determination of flow structure near the trailing edge at the tip of the blade and comparison with the images from the numerical simulation. All measurements were performed at equal operating and known ambient conditions.

The results show that the introduction of internal flow improved fan characteristics and reduced flow separation on the suction side of the blade. The increase of axial fan efficiency due to the introduction of internal flow also points to a more interesting technical solution from the economic point of view.

The tested axial fan presented in Fig. 2 had the diameter of 500 mm and was manufactured with 7 hollow blades [8]. The internal flow enters the internal radial flow passages of the hollow blades through the openings near the fan hub. The positioning of inlet and outlet slot was determined in a way that allowed maximal use of axial fan centrifugal force. The inlet hollow blade slot has a semicircle opening with the diameter of 40 mm (Fig. 1a). The outlet hollow blade slot on the trailing edge at the tip of the blade, where
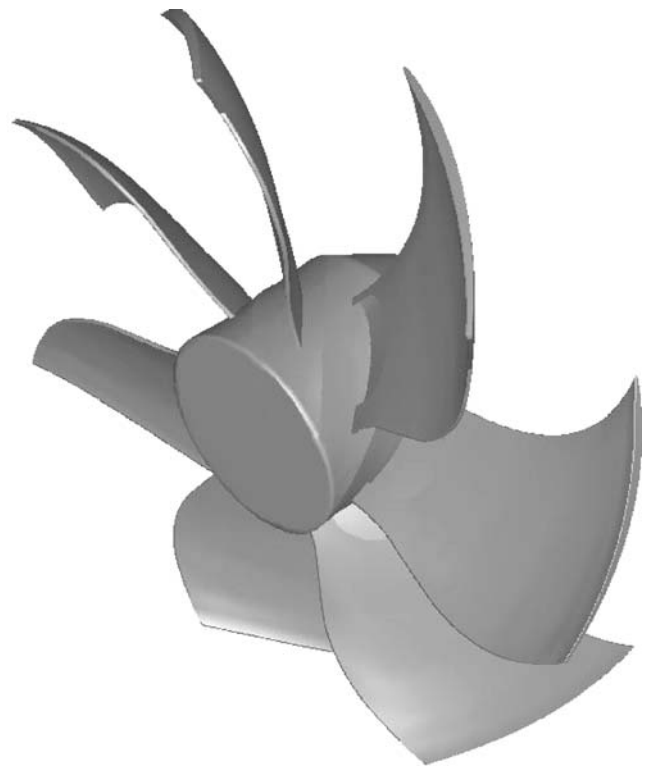
Fig. 2 Axial fan with self-induced hollow blades

the internal flow exits the blade internal passages, has the size of 20×1 mm (Fig. 1a). Hollow blades of the prototype axial fan were manufactured from fiber-reinforced composite materials to reduce the weight and deformation of hollow blades. The simplicity of the assembly was taken into account due to the possibility of serial production and the cost effective product with minimum complexity was achieved.

2 Numerical simulations

The method applied is based on the exactly defined geometry of the flow tract, which was given on the basic precedent selection and boundary conditions, which were set on machine's basic nominal properties. Fluid flow through the fan was treated in a steady condition. Simulations were carried out in five working points. In one series of simulations, internal flow, exiting through trailing edge slot was considered; in other series it was not. Software package Fluent 6.2.16 was used, where a set of Reynolds averaged Navier-Stokes equations was computed. Mass conservation equation (Eq. 1) and momentum conservation equation (Eq. 2) along with equations of $k - \omega$ SST turbulence model (Eqs. 3 and 4) are forming a closed system of equations [9]:

$$\frac{\partial \left(\bar{u}_j \right)}{x_j} = 0, \tag{1}$$

$$\frac{\partial \left(\rho \bar{u}_j \bar{u}_i \right)}{\partial x_j} = -\frac{\partial \bar{p}}{\partial x_i} + \frac{\partial}{\partial x_j} \left[\mu \left(\frac{\partial \bar{u}_i}{\partial x_j} + \frac{\partial \bar{u}_j}{\partial x_i} \right) - \rho \overline{u_i' u_j'} \right], \quad (2)$$

$$\frac{\partial \left(\rho k \bar{u}_j \right)}{\partial x_j} = \frac{\partial}{\partial x_j} \left[\Gamma_k \frac{\partial k}{\partial x_j} \right] + \tilde{G}_k - Y_k, \quad (3)$$

$$\frac{\partial \left(\rho \omega \bar{u}_i \right)}{\partial x_j} = \frac{\partial}{\partial x_j} \left[\Gamma_\omega \frac{\partial \omega}{\partial x_j} \right] + G_\omega - Y_\omega + D_\omega, \quad (4)$$

where $\tilde{G}_k$ is the turbulence kinetic energy source, because of velocity gradients, G_ω is the source of ω. Γ_k and Γ_ω are the effective diffusivity of k and ω. Y_k, Y_k and Y_ω represent dissipation of k and ω, because of turbulence. D_ω is the cross-diffusion term.

Meshes for the case with and without the internal flow were topologically equivalent. Computational domain was discretized with a structured mesh. To reduce the calculating time, only one interblade region (1/7 of the whole flow domain) was considered and periodic boundary condition was assumed at interfaces. A mesh with approximately 1 000 000 nodes was used, which was refined near the channel walls and along the fan blade – y^+ value was between 30 and 80. Discretization error was evaluated on a courser and finer mesh by monitoring the pressure upstream of the fan – an error based on Richardson extrapolation [9] of 0.5 per cent was calculated. With regard to the pressure development, convergence criterion was set on the inlet and velocity on the outlet from the computational domain. Parameters were always converging, when the residuals sum of transport equation in the entire computational domain was less than 1×10^{-3}. Finally, for convergence criterion, the situation was used, when the residuals decreased below 1×10^{-4}, for which approximately 350 iterations were needed. Iteration error was estimated to 0.05 per cent. Following calculating conditions were used:

- Flow: for turbulence, k-ω SST turbulence model was used.
- Boundary conditions: on the channel walls, fan blade and rotor, no slip boundary condition was assumed; On the inlet, air flow was defined ($\cong$ 3053, 4659, 5066, 5326, 5812 m^3/h); On the outlet, pressure was defined (1.013 bar).
- Fan rotating frequency was constant (1124 min^{-1}), fan rotation was described by the rotating reference frame model.

Air density was 1.225 kg/m^3 and dynamic viscosity was 1.79×10^{-5} Pas.

3 Experimental measurements

3.1 Measurements of integral characteristics

Measurements were performed for both versions with and without internal flow. To obtain comparable results, the measurements of integral characteristics were performed in accordance with standard [13, 14] at equal operating and ambient conditions and at equivalent fan operating points. The main sources of total measurement uncertainty for the measurements of integral characteristics [5] are uncertainty of measuring the rotating frequency, volume flow, pressure difference, temperature correction, humidity, etc. Overall measuring uncertainty is estimated to 2.6 per cent from the measured value and is in accordance with standard [13].

3.2 Measurements of local flow properties

Measurements of local flow properties were performed with a five-hole probe and computer-aided visualization. Measurements of both versions with and without internal flow were performed immediately one after another, in a way, which allows achieving minimal measurement uncertainty. Based on the results of measurements of integral characteristics, several axial operating points of the fan were selected. Local measurements presented in this paper were performed in optimal operating point at the outlet of the fan; at axial fan rotating frequency $n = 1124$ min^{-1} and static pressure difference $\Delta p_s = 91$ Pa. Figure 3 shows the measuring station scheme for measurements of local flow properties. The measuring station has a straight inlet flow section of $1.5 \cdot D$ and follows the recommendation in standard [14, 20].

In the optimal operating point of the axial fan, local flow measurements in 29 measuring points on blade radius were performed. Measurement points were selected on a line perpendicular to the axis at the distance of 5 mm behind the trailing edge of the blade. This allowed measurements across the entire trailing edge of the hollow blade, from the rotor hub to the blade tip. Measurement results in every measuring point were compared with the results from numerical simulation for the case with and without internal flow.

3.2.1 Velocity vector measurements with five-hole probe

Within the framework of local measurements, average velocity vectors were measured using a five-hole probe. Measurements using a five-hole probe were performed on a measuring station shown in Fig. 3. United Sensor Co. Type DA-187 probe was used, Fig. 3, point (6). For differential pressure measurements, differential pressure transmitters Endress+Hauser Deltabar S PMD75 were used, Fig. 3, point (13) and (16). Absolute pressure was measured with Vaisala PTB 220 while Vaisala HMT 331 transmitter was used for temperature and relative humidity measurement. We estimated the overall measurement uncertainty [11] for velocity vector measurements with five-hole probe to be 2.8 per cent for the measurement of velocity and $\pm 1°$ for the measurement of flow angles.

Fig. 3 Measuring station scheme for measuring local flow characteristics

1 - axial flow fan
2 - axial flow fan mesh
3 - wind tunnel with measured axial flow fan
4 - high-speed camera
5 - rotation direction of axial flow fan
6 - 5-hole pitot tube
7 - PC for control, acquisition, data storage 2
8 - inductive sensor
9 - rotational speed sensor
10 - illumination
11 - wind tunnel
12 - flow direction indication
13 - differential pressure transmitter 5
14 - axial flow fan with hollow blades, detail
15 - positioning table
16 - differential pressure transmitter 1-4
17 - PC for control, acquisition, data storage 1

3.2.2 Measurements with computer-aided visualization

The purpose of measurements with computer-aided visualization is to establish the form of internal flow at the exit from the blade. The results are compared to the results of numerical simulation. Measurements with computer-aided visualization were performed on a modified measuring station as in the case of measurements with five-hole probe, which is shown in Fig. 3. To visualize the internal flow, a passive tracer smoke from smoke tablets was used. Passive tracer was led through the hollow blade. Each time the selected blade passed the control volume, an image of passive tracer exiting the slot in the trailing edge was captured with a camera. Smoke generator cylinder was closed on one side. The smoke was directed to the center of the fan rotor. From there, a silicon tube attached to the fan hub directed the smoke towards the selected internal flow passage of the hollow blade. It must be emphasized that the smoke was not forced into the hollow blade – the inlet slot to the internal passage was constructed in a way to enable the external flow and smoke to enter freely into the internal flow passage due to the rotation of the fan. An assumption was made that smoke particles ideally follow the flow and that image intensity is proportional to smoke density [1]. Inlet smoke flow was evaluated with appropriate equipment for calculating intensity profiles [7]. Only one blade was equipped with the system for smoke generation.

Camera Dragonfly Express IEEE-1394b with Edmund Optics 75 mm Double Gauss, Fig. 3, point (4), lens was used for image acquisition. The camera was triggered with inductive proximity sensor Telemecanique Osiprox, Fig. 3, point (8), which was mounted in front of the electric motor of the fan. Recorded images had 8-bit grey level depth, resolution of 640×484 pixels, and were captured with shutter speed of 0.2 ms. The camera was triggered once per revolution of the

fan rotor in the same position. One image per revolution of the fan rotor was recorded. The camera was placed perpendicularly to the trailing edge surface of the hollow blade in the distance of 1 m from trailing edge of the axial fan. For illumination, a Vega Velum DC 150 W, Fig. 3, point (10), continuous flicker-free light source with randomized fibre light guide was used. Software package LabView was used for camera set-up, acquisition and storage of digital images. For each measurement point, 150 successive images were used for analysis, which proved to be satisfactory for the statistic evaluation [6] of smoke concentration at the outlet from the trailing edge slot at the tip of the blade. The number of images was limited by the time of uniform smoke generation. Overall measuring uncertainty of instantaneous passive tracer concentration was estimated to be 3.8 per cent of the measured value.

Algorithms for image analysis are discussed below [7]. Considering that digitalization was carried out with 8-bit B/W resolution, the value of the variable $E_p(i, j, t)$ in Eq. 5 giving the value of the grey intensity of a pixel (i, j) at time t is within the range:

$$E_p(i, j, t) \in \{0, \dots, 255\} \rightarrow \bar{E}_p(i, j). \tag{5}$$

Indices i and j of element E digital image present the position of the pixel in the image. Average intensity in the image $\bar{E}_p(i, j)$ was calculated. The results are shown in Sect. 4.2.2.

4 Results

4.1 Integral characteristics

The measured and numerical results of integral characteristics for the analyzed axial flow fan with hollow blade were

Fig. 4 Numerical and experimental results of axial fan static pressure and normalized efficiency for a case with and without internal flow

Legend:
- dps / with internal flow / exp
- dps / with internal flow / num
- eff / with internal flow / exp
- eff / with internal flow / num
- dps / without internal flow / exp
- dps / without internal flow / num
- eff / without internal flow / exp
- eff / without internal flow / num
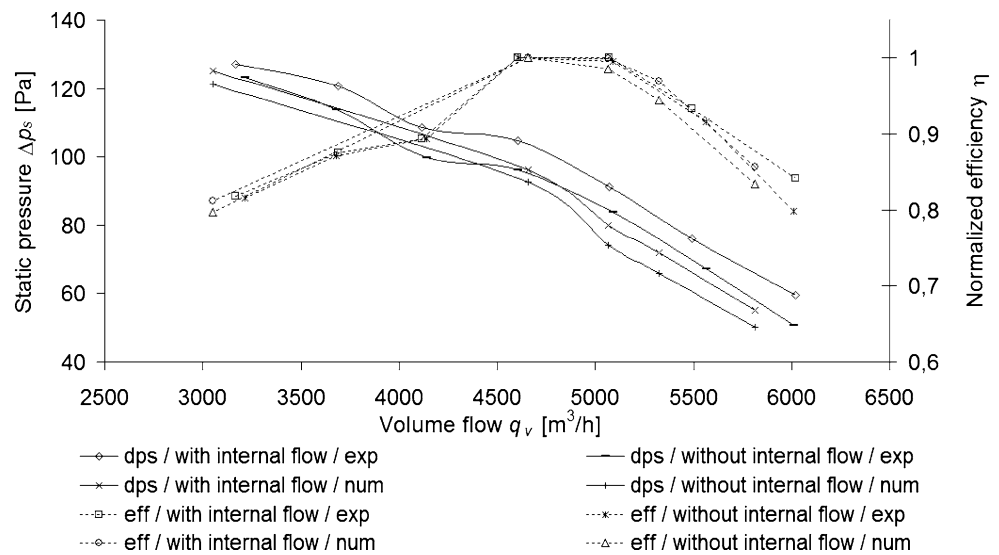
compared. Figure 4 shows numerical and experimental results for integral characteristics of the axial fan for both versions with and without internal flow in dependence of volume flow. Normalized efficiency in Fig. 4 is given as a ratio between efficiency and its own maximal value of efficiency.

Results of numerical simulation agree with measurement results for the normalized efficiency. For the static pressure difference, numerical model follows the static pressure of measurement results, otherwise deviations are higher. Higher deviation can be seen probably due to the result of overestimated prediction of flow separation on the trailing edge of the blade.

The static pressure difference is present through the complete operating range and is higher for the case with internal flow through the trailing edge slot at the tip of the blade. When internal flow was introduced, an increase in normalized efficiency and static pressure difference (up to 6.5 per cent) was observed (Fig. 4).

We assume that qualitative changes of flow structures over axial cascade appear between both cases. It can be assumed that the blade wake is reduced, which consequently leads to shifting of the characteristic towards larger values of flow in the complete operating range of the axial fan. For this reason, detailed local measurements in the region of optimal operating point were performed near the trailing edge slot.

4.2 Local characteristics

The measurements of local characteristics were performed with a five-hole probe and computer-aided visualization, as explained in Sect. 3. To estimate the direction of internal flow, graphical presentation of internal flow through hol-
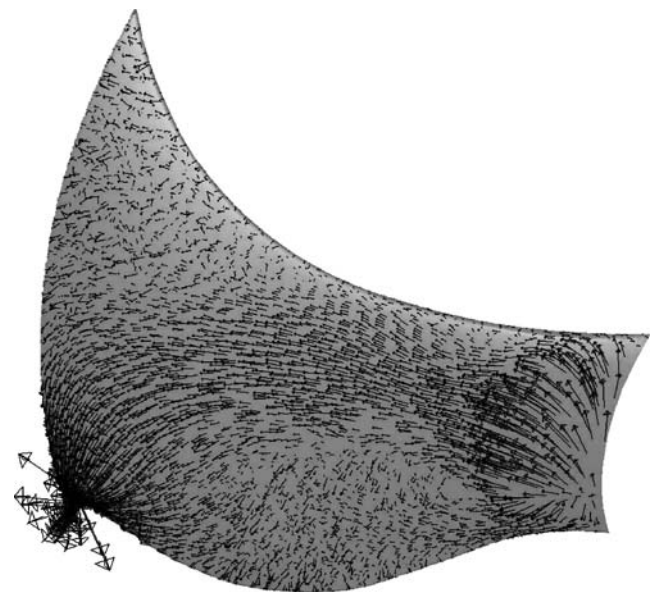
Fig. 5 Numerical simulation of relative velocity u_j of hollow blade internal flow in optimal working point at $\Delta p_s = 91$ Pa

low blade in Fig. 5 is presented. Figure 5 shows relative internal flow velocity of the hollow blade in optimal working point at $\Delta p_s = 91$ Pa made with numerical simulation by introducing the graphical presentation of velocity field in the internal flow passage and on the region of the trailing edge slot at the tip of the hollow blade. Internal flow enters the internal radial flow passage all the way to the trailing edge at the tip of the blade, where internal flow exits through the trailing edge slot. A free jet flow forms, when internal flow exits through the trailing edge slot and mixes with the surrounding ambient fluid. Ambient fluid particles are carried in axial direction along the free jet fluid flow,

consequently, fluid mass flow increases. Numerical simulation in the optimal operating point of the axial fan shows that the internal flow velocity u_j, when it exits through the tip trailing edge slot, is estimated to 28.1 m/s, compared to relative external velocity w, estimated to 24.9 m/s, and is greater ($u_j > w$) meaning that internal flow forces the external flow in its direction. At this point, it is important to emphasize that the external flow velocity w, obtained from the velocity vectors, presents the velocity in the far-field region from the blade wall and proportionally reduces in direction towards the blade wall [18]. Consequently, it can be assumed that internal flow in the near wall region has an even higher influence towards the external flow; therefore, it is assumed that velocity $u_j \gg w$. The internal flow is self-induced as no energy is required, and the only driving force is rotation of the fan. The internal flow is mainly driven by the centrifugal forces resulting from the rotation of the axial fan. Using these modifications, the reduction of adverse flow conditions near the trailing edge at the tip of the hollow blade, boundary layer reduction on the blade suction side and the reduction of flow separation was achieved, which enabled increased local energy conversion and improved fan characteristics (Fig. 4).

4.2.1 Local velocities

The results in previous section show that in the case with internal flow qualitative changes of flow structures over axial cascade appear. Consequently, this led to shifting of the characteristic towards higher static pressure in the complete operating range of the axial fan. For this reason, detailed local measurements in the region of optimal operating point were performed from the hub of the axial fan to the trailing edge of the hollow blade.

Numerical results were compared with experimental results of measurements with a five-hole probe, which were performed with and without internal flow in the optimal operating point. Results of measurements with a five-hole probe are in agreement with the results obtained by numerical simulation. Both results confirmed that the introduction of internal flow has a positive influence on the flow through the fan.

Figure 6 presents axial velocity and velocity angle α, which is the angle between axial and tangential velocity, Fig. 7 presents tangential velocity and Fig. 8 presents radial velocity.

Figure 6 shows that in the case with internal flow the axial velocity on the trailing edge of the blade near the tip from 210 to 240 mm and as well as on radius of 70 and 100 mm increases. It is interesting that by introducing the internal flow more beneficial conditions near the hub of the fan (from 70 to 100 mm) were generated as well. Velocity increases in the near hub region as a result of a more plausible fluid flow, because a part of external flow is sucked into the internal radial flow passage of the hollow blade. This reduces the generation of vortices near the fan hub which is usual for this fan type, and the used method of attachment of blades to the hub by riveting. In the middle of the blade span (from 100 to 200 mm from the axis of the fan), velocity and angle α deviations are not distinctive.

Also, a change in velocity angle α is substantial as it increases on the trailing edge of the blade near the tip and decreases in the region near the hub of the fan. This points to the fact that the flow direction is changed and that the airflow in the case of internal flow better follows the profile of the fan blade.

We get similar results for the case with internal flow in Fig. 7, where tangential velocity on the trailing edge of the hollow blade near the tip increases. This occurs because the

Fig. 6 Axial velocity and angle α for the optimal operating point of the axial fan at $\Delta p_s = 91$ Pa
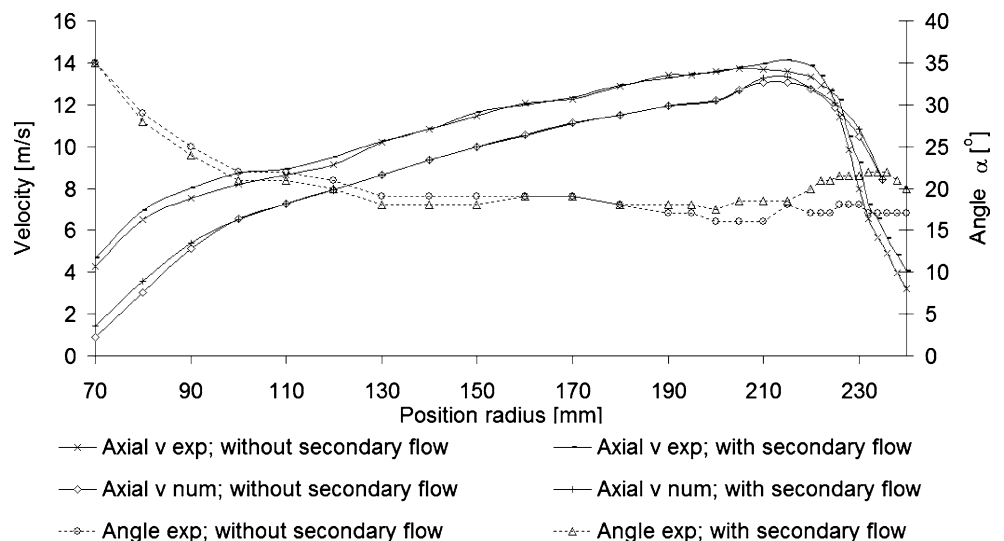
Fig. 7 Tangential velocity for the optimal operating point of the axial fan at $\Delta p_s = 91$ Pa

- Tan v exp; without secondary flow
- Tan v exp; with secondary flow
- Tan v num; without secondary flow
- Tan v num; with secondary flow
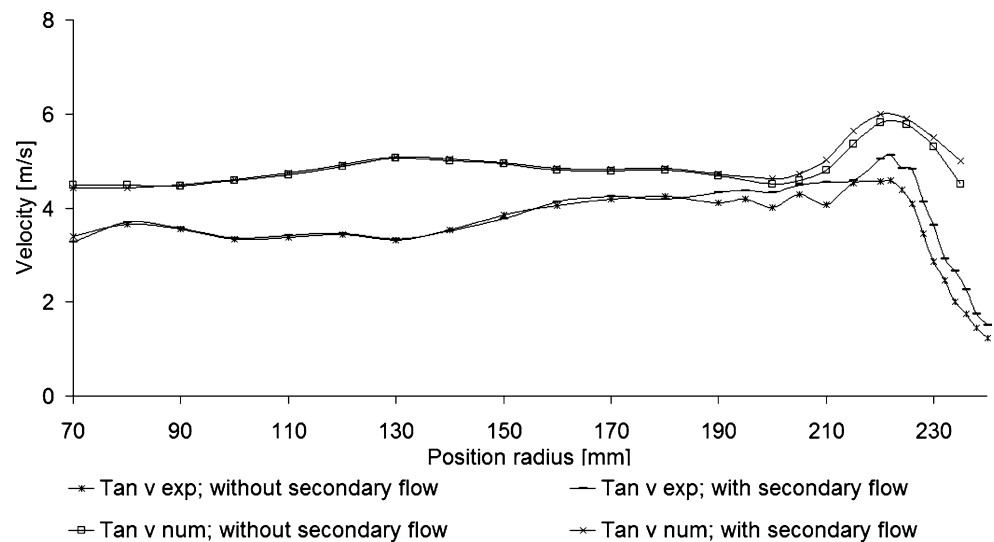
Fig. 8 Radial velocity for the optimal operating point of the axial fan at $\Delta p_s = 91$ Pa

- Rad v exp; without secondary flow
- Rad v exp; with secondary flow
- Rad v num; without secondary flow
- Rad v num; with secondary flow
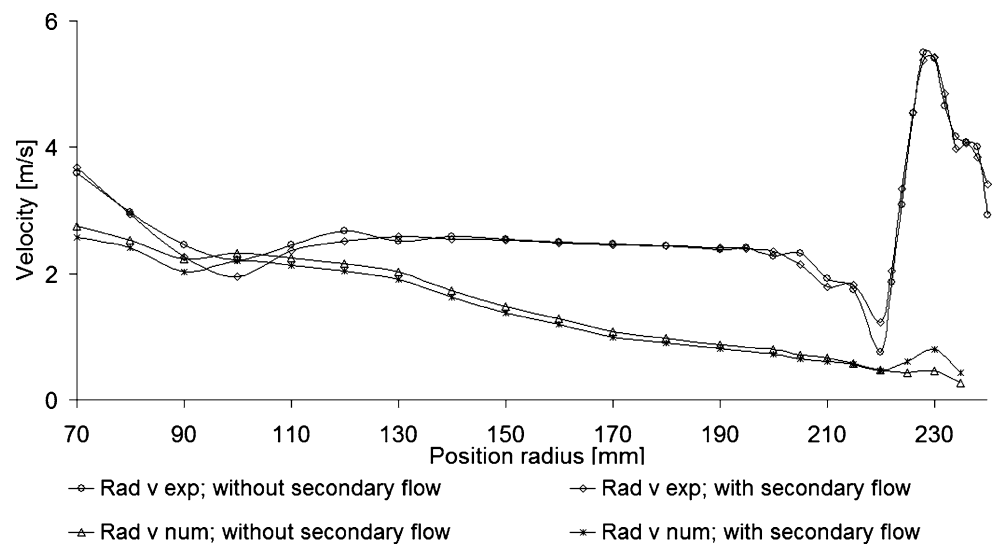
internal flow adds energy to the external flow and consequently contributes to the preservation of flow direction. As a direct result, flow separation from the suction side of the hollow blade and the thickness of the boundary layer are reduced which leads to higher fan efficiency.

Figure 8 shows that in the case with internal flow the radial velocity on the trailing edge of the blade near the tip as well as on radius of 90 and 100 mm decreases. These changes are a result of flow passing into the internal flow passage. In the middle of the blade span (from 100 to 200 mm from the axis of the fan), velocity is not distinctive.

In the conclusion of these results it can be pointed out that increased velocity was obtained due to the introduction of the hollow blade internal flow. It can be assumed that at the tip trailing edge, where mixing of external and internal flow is taking place, stabilization of flow structures is expected.

4.2.2 Local passive tracer concentrations

The results of computer-aided visualization were compared with the results of the numerical simulation. The results are shown only for the case of fan with the enabled internal flow in optimal operating point. Measurements without internal flow were not performed as the internal passage was used as the supply of smoke. The purpose of the measurement was to present the shape and flow direction of the jet as it exits through the slot and to confirm the results of the numerical simulation. Results shown in Fig. 9a and b gave the view of local flow behavior in the region of the trailing edge of the hollow blade. Figure 9a shows internal flow from the numerical simulation. Figure 9b shows smoke intensity contour of internal flow after the exit from the slot measured with computer-aided
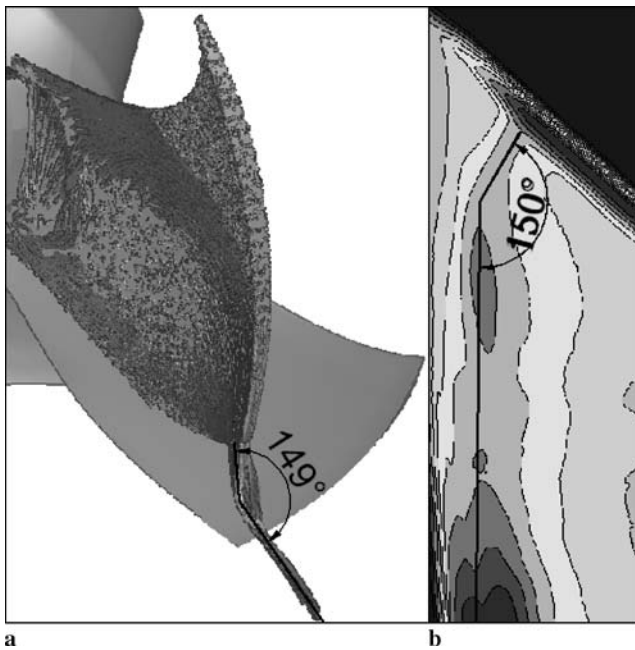
Fig. 9 Internal flow contours in optimal operating points at $\Delta p_s = 91$ Pa. **a** numerical model of internal flow, **b** computer-aided visualization image of internal flow

visualization. The contour presents the intensity of outlet which exits through the trailing edge slot of the hollow blade.

Internal flow at the exit from the slot mixes with the external flow and generally preserves the direction and shape. External flow is forced to follow the path of internal flow; hence the mass flow in the jet direction increases. Comparing the numerical and experimental results, it can be seen that there is a comparison of the obtained results, showing the flow direction changes and the point where flow changes its path. In conclusion to this analysis, we confirmed the numerically predicted path of internal flow with computer-aided visualization.

5 Conclusions

The paper presented the introduction of flow through the hollow blades of the axial fan. With the help of different measuring techniques, effects of the internal flow on the hollow blade flow field were determined. Increased velocity was obtained from the internal flow passing through hollow blades. The biggest difference occurs near the hollow blade's tip trailing edge, where internal flow exits from trailing edge slot at the tip of the hollow blade. By introducing the internal flow, more beneficial conditions near the hub of the fan are generated as well. Axial and tangential velocities increase in the region near the hub as a result of a more plausible fluid flow as a part of external flow, en-

tering the internal flow passage of the hollow blade. This reduces the generation of vortices near the fan hub, which is usual for this type of fan and for the used method of attaching the blades to the hub by riveting. In the middle of the blade radius, velocity remains practically unchanged. Therefore, it is assumed that the external flow field changes and follows the blade contour better – the flow separation near the trailing edge at the tip of the hollow blade on the suction side minimizes. The beneficial influence also reflects in the integral characteristic, where up to 6.5 per cent increase in static pressure difference was achieved. The suitability of using an axial flow fan with hollow blade is obvious.

The hollow blade will undergo additional development and research. With the hot-wire anemometry, local velocity should be measured and compared with the measurements with five-hole probe, presented in the paper. In addition, acoustic measurements on both cases of the axial fan with and without internal flow should be performed. Finally, the aim is to manufacture final product of the axial fan with hollow blades, using polyamide material with selective laser sintering technology.

References

1. Balu M, Balachandar R, Wood H (2001) Concentration Estimation in Two-Dimensional Bluff Body Wakes Using Image Processing and Neural Networks. J Fluid Struct 8(2–3):121–140
2. Bleier FP (1997) Fan Handbook Selection, Application and Design. McGraw Hill, New York
3. Batchelor GK (2000) An Introduction to Fluid Dynamics. Cambridge University Press, Cambridge
4. Borello D, Hanjalic K, Rispoli F (2007) Computation of tip-leakage flow in a linear compressor cascade with a second-moment turbulence closure. Int J Heat Fluid Flow 28(4):587–601
5. Coleman HW, Steele WG (1989) Experimentation and Uncertainty Analysis for Engineers. John Wiley & Sons Inc., New York
6. Dular M, Bachert B, Stoffel B, Širok B (2004) Relationship between Cavitation Structures and Cavitation Damage. Wear 11:1176–1184
7. Eberlinc M, Dular M, Širok B, Lapajne B (2008) Influence of Blade Deformation on Integral Characteristic of Axial Flow Fan. J Mech Eng 3(54):159–169
8. Eberlinc M, Širok B, Hočevar M, Dular M (2007) Axial Turbine Machine Hollow Blade with Internal and External Flow Field. The Slovenian Intellectual Property Office, Patent No. P 200700271, Ljubljana, Slovenia
9. Ferziger JH, Perić M (2002) Computational Methods for Fluid Dynamics, 3rd Edition. Springer, Berlin
10. Garg VK (2002) Heat Transfer Research on Gas Turbine Airfoils at NASA GRC. Int J Heat Fluid Flow 23:109–136
11. Gonsalez JC, Arrington EA (1999) Five-Hole Flow Angle Probe Calibration for the NASA Glenn Icing Research Tunnel. Dynacs Engineering Company, Inc, Brook Park, Ohio
12. Hinze JO (1959) Turbulence: an Introduction to its Mechanism and Theory. McGraw-Hill, New York
13. ISO 5801 (2007) Industrial Fans
14. ISO 5167 (2003) Measurement of fluid flow